Chinese Science Bulletin

Hydrothermal plume anomalies along the Central Indian Ridge

ZHU Jian[1], LIN Jian[2†], GUO ShiQin[3] & CHEN YongShun[1]

[1] Department of Geophysics, School of Earth and Space Sciences, Peking University, Beijing 100871, China;
[2] Department of Geology and Geophysics, Woods Hole Oceanographic Institution, Woods Hole, MA 02543, USA;
[3] China Ocean Mineral Resources R&D Association, Beijing 100860, China

Water column turbidity and temperature were investigated along the Central Indian Ridge (CIR) from 25°19′S to 23°48′S during a December 2005 cruise on board Chinese R/V DayangYihao. Measurements were made using NOAA's MAPR (Miniature Autonomous Plume Recorder) sensors during CTD casts, TV grabber operations, and tow-yo profiles, yielding the following results on hydrothermal plume anomalies: (1) Strong hydrothermal turbidity and temperature anomalies were recorded over the previously discovered Kairei (25°19.2′S, 70°02.4′E) and Edmond (23°52.7′S, 69°35.8′E) vent fields, with the plume anomalies concentrated at depths of 2150—2300 m and 2700—2900 m, respectively. The maximum height of the turbidity anomalies near the Kairei vent field recorded in December 2005 was slightly below 2100 m, which is consistent with the plume depth measured in June 2001, indicating that the Kairei plume may have maintained its buoyancy flux in the intervening 4.5 years. (2) The water column beneath the Kairei plume has background anomalies of about 0.005ΔNTU, whereas no such background turbidity anomalies were observed below the Edmond hydrothermal plume. (3) No visible turbidity anomalies were detected from 24°42′S to 24°12′S including the Knorr Seamount. Thus 24°12′S marks the southern end of the hydrothermal plume. (4) Significant turbidity anomalies were observed at four individual sections from 24°12′S to 23°56′S at the depth of 2500—3000 m along the eastern rift valley wall. Whether the individual sections of anomalies are connected is still unknown due to the absence of data at the intervening gaps. If the four sections are connected with each other and are linked to the Edmond vent field farther to the north, the total along-axis length of the plume anomaly would be more than 37 km, implying a plume incidence value p_h of 0.38, greater than the predicted p_h of 0.21—0.25 based on the spreading rate of the Central Indian Ridge.

Central Indian Ridge, hydrothermal plumes, Kairei and Edmond vent fields, turbidity anomalies, MAPR

The first Chinese global expedition on board R/V DayangYihao, the DY105-17A cruise, was conducted from August 2005 to January 2006 to explore and investigate hydrothermal vents along mid-ocean ridges in the Pacific, Atlantic, and Indian Oceans. In December 2005, we surveyed the Central Indian Ridge (CIR) immediately north of the Rodriguez Triple Junction (RTJ). Multi-disciplinary investigations were conducted near the Kairei and Edmond vent fields, which were first discovered and sampled in 2000[1] and 2001[2], respectively. We also surveyed a previously little studied region between the Edmond vent field and immediately south of the Knorr Seamount. This paper reports the hydrothermal plume anomalies detected during this cruise and discusses their implications.

1 Geological setting

The Central Indian Ridge is an intermediate spreading

Received November 2, 2007; accepted March 4, 2008
doi: 10.1007/s11434-008-0208-6
†Corresponding author (email: jlin@whoi.edu)
Supported by WHOI Deep Ocean Exploration Institute and Cecil H. and Ida M. Green Technology Innovation Awards (J. Lin) and the Chinese Ocean Mineral Resources R&D Association (J. Chen)

system with a full spreading rate of 50—60 mm/a[3]. It is a branch of a ridge-ridge-ridge system centered at the RTJ (Figure 1(a)). The ridge axis has an overall trend of NNW[4] (Figure 1). Two known hydrothermal vent fields, Kairei and Edmond, are located within the southernmost part of the CIR.

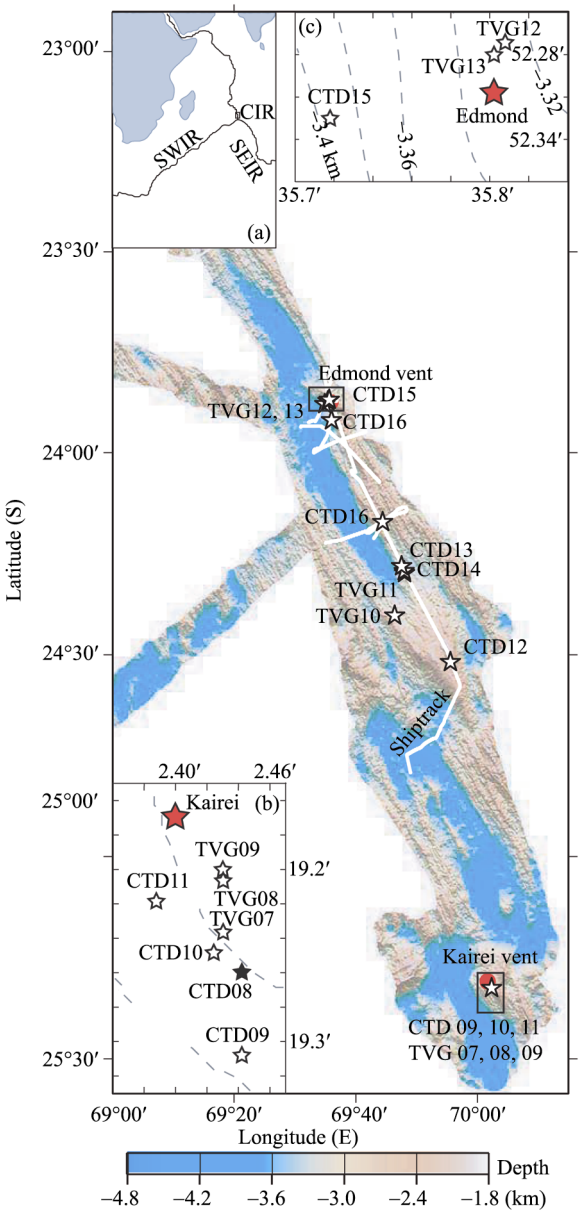

Figure 1 Multi-beam bathymetric map of the working area at the Central Indian Ridge. The base map is from Figure 1 of Gallant and Von Damm[6]. The white lines are tow-yo profiles and the white stars are *in-situ* CTD and TVG stations. (a) Sketch of the three branches of the Rodriguez Triple Junction, i.e., the Central Indian Ridge (CIR), Southeast Indian Ridge (SEIR), and Southwest Indian Ridge (SWIR). (b) Stations near the Kairei vent field (red star). The open stars indicate the station measurements made in our December 2005 cruise and the solid star is the CTD08 cast in Rudnicki and German's June 2001 survey[9]. (c) Stations near the Edmond vent field (red star). In (b) and (c), the dashed lines show bathymetry contours.

The Kairei vent field (25°19.2′S, 70°02.4′E) was first discovered by scientists from JAMSTEC (Japan Agency for Marine-Earth Science and Technology) using the ROV Kaiko on board R/V Kairei in August 2000[5]. It is located at a 20-km-long ridge segment immediately north of the RTJ. The hydrothermal venting occurs high on the eastern rift valley wall, where the seafloor is 2420—2460 m, and is about 1800 m shallower than the maximum rift valley depth[2]. The active vent sites of high-temperature (306°—365℃) are situated on the southwestern flank of the Hakuho Knoll, which has a topographic slope of 10°—30°[6], trends WNW, extends about 80 m along the rift wall, and is about 30 m wide[2].

The Edmond vent field (23°52.7′S, 69°35.8′E) is about 160 km NNW from the Kairei vent field. The Edmond vent field also occurs on the eastern rift valley wall and at water depth of 3290—3320 m. The main area of the high-temperature vent field is about 40 m^2[6]. The ridge segments hosting the Kairei and Edmond vent fields are both associated with rift valleys, which are typical of the axial ridge morphology on hotspot-free intermediate spreading ridges such as the Gorda Ridge (60 mm/a) and Galapagos Spreading Center west of 97°W (46 mm/a)[7]. Both the Edmond and Kairei hydrothermal vent fields do not occur at the center of the ridge axis, but are instead located at a distance of greater than 6 km to the east of the spreading axis[6]. Both vent fields occur on the inside corners of left-lateral offset discontinuities of the ridge axis. The Kairei vent field is at the center of the segment, whereas the Edmond vent field is at the northern end of the segment.

2 Methods

Continuous turbidity measurements were made using six Miniature Autonomous Plume Recorders (MAPRs) on loan from NOAA. Our survey consisted of 16 *in situ* profiling stations including 9 CTD casts, 7 TVG casts, and 6 tow-yo profiles both along the ridge east wall and across the ridge axis (Figure 1 and Table 1). MAPR instruments were clamped on a co-axial cable at 20 m above a CTD rosette and 50 m above a TV-grabber, with a constant spacing of 20 m. In tow-yo profiles, six MAPRs were installed 20 m above a camera tow vehicle and the spacing between the MAPRs was 70 m.

Table 1 MAPR deployment information

Station No.	Start			End		
	Location	Water depth (m)	Date-Time (GMT)	Location	Water depth (m)	Date-Time (GMT)
CTD09	25°19.4′S, 70°02.4′E	2488.6	12/13, 21:15:25	25°20.7′S, 70°02.2′E	2893.9	12/13, 23:59:25
CTD10	25°19.3′S, 70°02.4′E	2454.0	12/14, 08:10:40	25°20.3′S, 70°02.1′E	2807.7	12/14, 11:13:05
CTD11	25°19.2′S, 70°02.4′E	2452.1	12/14, 12:06:20	25°19.2′S, 70°02.4′E	2466.6	12/14, 14:05:10
CTD12	24°31.1′S, 69°55.6′E	2259.1	12/17, 18:31:10	24°31.7′S, 69°52.2′E	2903.7	12/17, 20:34:00
CTD13	24°16.9′S, 69°47.7′E	3178.8	12/17, 22:47:40	24°17.0′S, 69°47.7′E	3138.3	12/18, 02:23:45
CTD14	24°17.7′S, 69°48.0′E	3124.6	12/18, 03:29:30	24°18.6′S, 69°44.9′E	3153.7	12/18, 06:39:05
CTD15	23°52.7′S, 69°35.7′E	3373.5	12/19, 17:05:25	23°52.3′S, 69°34.2′E	3492.2	12/19, 19:56:30
CTD16	23°55.2′S, 69°35.9′E	3116.6	12/20, 08:02:25	23°55.0′S, 69°34.4′E	3657.0	12/20, 10:51:55
CTD17	24°10.5′S, 69°44.3′E	3344.3	12/20, 13:20:25	24°10.8′S, 69°41.9′E	3943.3	12/20, 16:11:35
TVG07	25°19.2′S, 70°02.4′E	2433.2	12/13, 17:08:55	25°19.8′S, 70°02.4′E	2683.8	12/13, 20:06:20
TVG08	25°19.3′S, 70°02.4′E	2458.8	12/14, 02:39:35	25°19.9′S, 70°01.4′E	2824.7	12/14, 07:25:25
TVG09	25°19.2′S, 70°02.4′E	2432.4	12/17, 05:06:15	25°19.7′S, 70°02.4′E	2628.4	12/17, 07:59:50
TVG10	24°24.1′S, 69°46.4′E	2625.6	12/17, 14:06:15	24°24.4′S, 69°45.3′E	3052.4	12/17, 16:36:10
TVG11	24°17.7′S, 69°48.2′E	3115.8	12/18, 08:16:15	24°16.9′S, 69°46.8′E	3381.8	12/18, 15:34:15
TVG12	23°52.8′S, 69°35.3′E	3542.5	12/20, 18:45:25	23°53.1′S, 69°34.0′E	3536.4	12/21, 01:06:25
TVG13	23°52.7′S, 69°35.8′E	3328.2	12/21, 01:58:30	23°53.2′S, 69°34.6′E	3509.1	12/21, 05:09:55
T1	23°53.7′S, 69°36.2′E	3442.3	12/15, 12:42:20	24°13.0′S, 69°43.0′E	3416.9	12/16, 00:10:10
T2	24°09.4′S, 69°43.5′E	3017.1	12/16, 03:53:45	24°47.7′S, 69°49.1′E	3480.8	12/17, 00:39:50
T3	24°10.3′S, 69°44.6′E	2948.4	12/18, 18:46:20	24°13.7′S, 69°35.0′E	2680.7	12/19, 05:08:20
T4	24°04.7′S, 69°44.0′E	2421.7	12/19, 08:03:05	23°56.5′S, 69°30.9′E	3528.0	12/19, 15:25:20
T5	23°52.7′S, 69°35.0′E	3566.2	12/20, 00:29:10	23°55.9′S, 69°32.2′E	3786.0	12/20, 06:36:20
T6	23°48.7′S, 69°35.7′E	2864.6	12/21, 09:21:45	23°57.3′S, 69°41.6′E	2709.1	12/22, 00:18:50

CTD refers to CTD stations; TVG to TVG deployments; T to tow-yo profiles.

2.1 Turbidity data processing

The MAPR sensor measures water column turbidity by a light-backscattering sensor[8]. The sensor measurement range is 0—5000 mV with the sensitivity of 0.01 mV. The sampling interval is 5 s. The raw voltage outputs in volt are directly equivalent to Nephelometric Turbidity Units (NTU). The turbidity data were processed to yield the anomalous NTU (i.e., ΔNTU) based on the following three steps:

(1) Removal of the isolated spikes. Spikes in turbidity signals often result from isolated large particles in the water column. We filter out spike point signals beyond the ±1 standard deviations from a moving average of every 11 points in the time-series record, being consistent with previous studies (Sharon Walker, 2008, personal communication).

(2) Between MAPR instrument calibration. For each MAPR we calculate the average turbidity measurement (without spikes) from all deployments at depths of 1000—1200 m, where no plume signals exist. Assigning any MAPR as a reference sensor (MAPR09 in this case), we calculated the differences in the average values at 1000—1200 m between other five MAPRs and the reference MAPR and define them as instrument calibration factors.

(3) Calculation of turbidity anomaly. Within the survey area, the MAPR sensors show instrumental values of about 0.018 ΔNTU for places where no turbidity anomaly exist. We subtracted this constant instrumental value from the turbidity measurements.

2.2 Sensor location estimation

The MAPR sensor locations during both *in situ* and tow-yo deployments were estimated from the seafloor topography and the ship location, the latter of which was determined by shipborne Seastar differential GPS. The errors in estimating sensor location result mainly from the fact that the sensor-carrying vehicle, which is relatively light-weight, was towed significantly behind the ship during tow-yo surveys. However, for most of the time the tow vehicle was required to be within 50 m from the bottom topography with the aid of a near-bottom altimeter mounted on the tow vehicle. Thus in the absence of detailed data on the wire-out length of the sensor-carrying tow vehicle, we simply shift the vehicle and sensor location to match the topography since the vehicle is mostly within 50 m from the bottom. In Figure 2 the grey line shows the topography along a survey line, the dashed black line denotes the uncorrected sensor track,

and the solid black line is the corrected sensor track. Each symbol pair shows the uncorrected (A—G) and the corresponding corrected (A'—G') sensor locations, respectively.

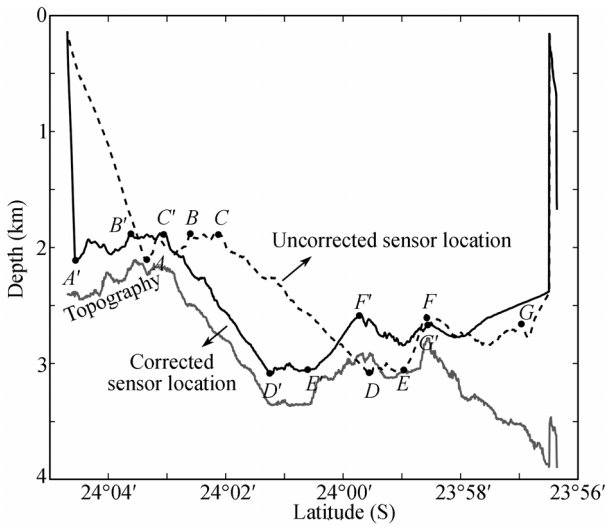

Figure 2 Diagram showing an example of sensor location correction. The gray line is the topography recorded by a ship multi-beam bathymetry system. Point A on the dashed black line shows the original, uncorrected sensor location. Point A' on the solid black line is the estimated sensor location by requiring the sensor-carrying tow vehicle to be within 50 m from the bottom topography. Each symbol pair represents the uncorrected and corrected locations, respectively. Points A' to G' represent the corrected sensor positions after shifting from the original uncorrected sensor positions A to G.

3 Results and discussion

Figures 3—6 show the turbidity and temperature anomalies recorded by MAPR sensors at *in situ* stations and along tow-yo profiles.

3.1 The Kairei vent field

Six *in situ* deployments were conducted near the Kairei vent field, including CTD09-11 and TVG07-09. The *in situ* deployment stations are shown in Figure 1(b) with circles. Turbidity anomalies were detected during all casts (Figure 3). The typical nose-shaped particle plume is about 100—150 m thick and is mainly concentrated at a depth interval of 2150—2300 m. The water column below the plume is associated with local background turbidity anomalies of about 0.005 ΔNTU relative to the water column above the plume. The maximum turbidity anomaly was recorded during TVG07 deployment (Figure 3(d)) with a maximum anomaly of about 0.08 ΔNTU at the depth of 2230 m. The vertical thickness of the plume is about 100 m with the upper boundary at 2170 m. A distinct temperature spike of 0.05℃ was detected in TVG08 deployment at the depth of 2350 m, where sharp turbidity anomaly spikes also appeared with a maximum value of 0.03 ΔNTU (Figure 3(e)). Both the turbidity and temperature spikes indicate that the sensor was very close to an active hydrothermal vent.

We choose the downcast CTD09, during which the measured plume was the highest among the six casts, to compare with the measurements of Rudnicki and German made in June 2001[9] (Figure 4). The distance between the ship locations of the 2001 and 2005 CTD stations is about 85 m. The maximum height of the plume during the December 2005 survey was slightly below 2100 m, which is less than 30 m from the maximum plume height measured in June 2001. In plume flux calculations, the calculated buoyancy flux is much more sensitive to the observed plume height (to the 4th power), than to the vertical density gradient of the seawater (to the power of 3/2)[10]. Thus the result of comparable plume heights observed in the 2001 and 2005 surveys suggests that the Kairei hydrothermal vent may have maintained its buoyancy flux during the intervening 4.5 years.

3.2 The Edmond vent field

Three *in situ* deployments were conducted above the Edmond vent field (Figure 1(c)). The vertical thickness of the hydrothermal plume layer is about 400 m and the plume is spreading at a depth interval of 2700—2900 m. The maximum turbidity anomaly of the nose-shaped plume is about 0.13 ΔNTU, which is about 1.5 times the value of the maximum turbidity anomaly observed in the plume above the Kairei vent. At station TVG12, both turbidity and temperature sensors recorded sharp spikes at a depth interval of 3100—3200 m (Figure 5(b)). The maximum turbidity and temperature anomalies are up to 0.54 ΔNTU and 0.21℃, respectively. In contrast to the existence of background turbidity anomalies beneath the Kairei plume, there were no observable turbidity anomalies beneath the Edmond hydrothermal plume.

3.3 Survey between the Edmond vent field and south of the Knorr Seamount

Turbidity and temperature measurements were made from 24°42′S to 23°52′S both along the eastern rift valley wall and across the ridge axis. Figure 6 shows the results of turbidity measurements along each profile. Values less than 0.01 ΔNTU are represented by the light gray, while values greater than 0.04 ΔNTU are saturated

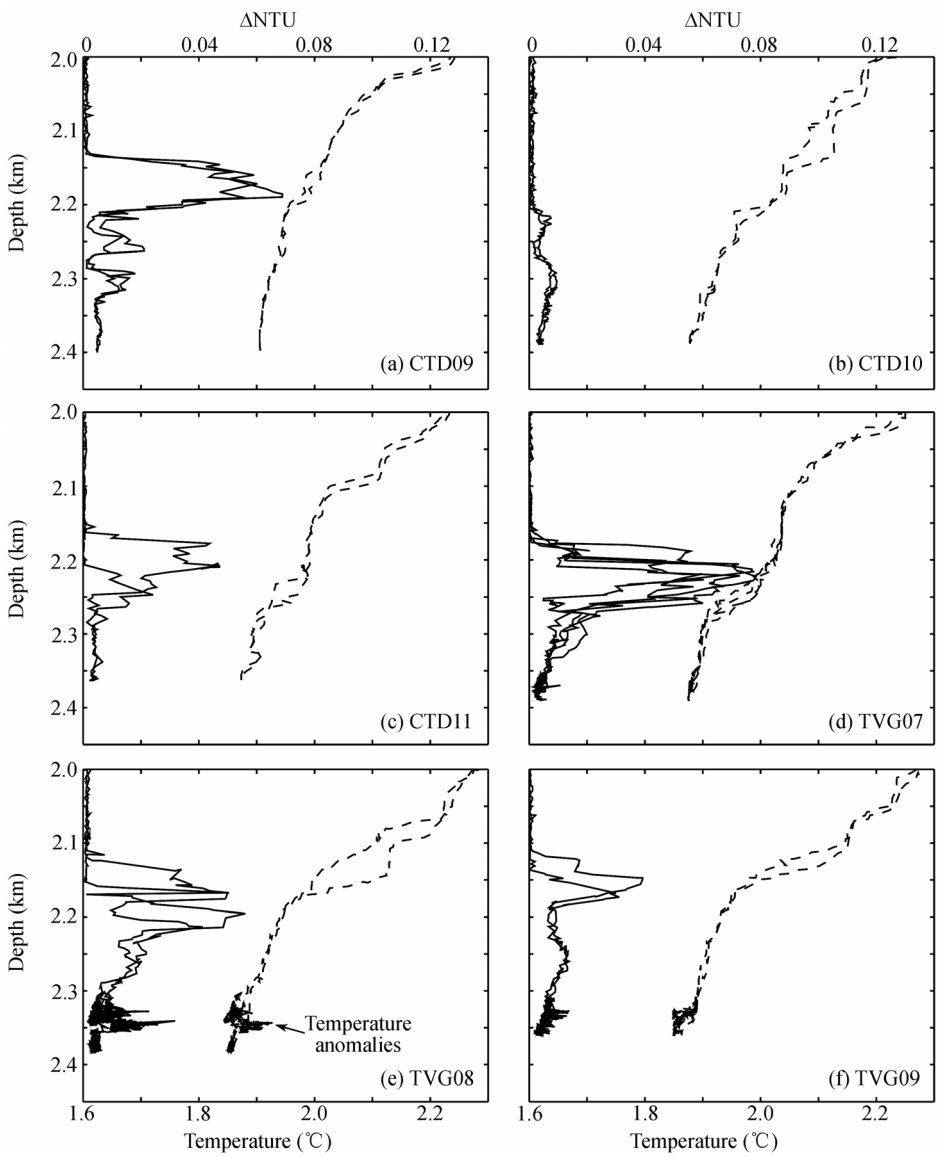

Figure 3 Results of *in situ* MAPR station measurements near the Kairei vent field. The solid lines show the turbidity anomalies and the dashed lines show temperature measurements. The black arrow in (e) indicates obvious temperature spikes.

in red. The gray shaded areas show the seafloor topography as determined by a shipboard SIMRAD multibeam bathymetry system. Our bathymetry data collected in the 2005 cruise match very well the online open database (http://www.marine-geo.org) within the survey area where we had good bathymetric records. All the MAPR sensor tracks were corrected to follow the variations in topography. Near-bottom water columns were relatively free of turbidity anomalies from 24°42′S to 24°12′S (Figure 6(a) and (b)). No turbidity anomalies greater than 0.01 ΔNTU were observed in this region in both *in situ* stations and the tow-yo profiles along the rift valley wall (Figure 6(a)). The Knorr Seamount near 24°30′S is as shallow as 2100 m but was not associated with noticeable turbidity anomalies, indicating that there were not active vents near this volcanic feature at the time of our December 2005 survey.

Within the region from 24°12′S to 23°50′S, significant turbidity anomalies were observed at four sections, *A*—*D* (Figure 6(b)), from the depth of 2500 to 3000 m. In section A, turbidity anomalies were recorded at CTD17 station and in the along-axis profile (Figure 6(b)), as well as in the across-axis profile (Figure 6(c)). The turbidity anomalies are concentrated at a depth interval of 2600—3000 m with maximum anomalies of greater than 0.025 ΔNTU. This anomaly extends about

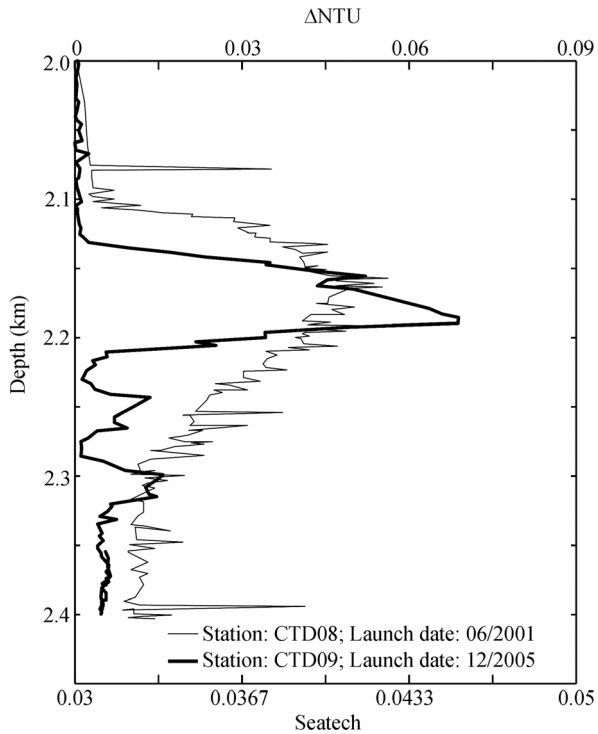

Figure 4 Comparison of turbidity anomalies near the Kairei vent field between measurements made in December 2005 and June 2001. The gray thin curve is the turbidity measurement in June 2001 from Rudnicki and German[9]. The black thick line is our December 2005 measurement during CTD09 deployment, for which the observed plume is the highest among all six casts. Note that the absolute turbidity anomaly values of the December 2005 and June 2001 surveys are not comparable because different sensors were used.

1.85 km along the rift valley wall and spreads at least 2 km towards the rift valley (Figure 6(c)). The axial rift valley at this location is deeper than 3500 m, which appears to be too deep to be the location of a turbidity source for a plume rising to the depth of 2600—3000 m. From this geometrical consideration, we suggest that the observed turbidity anomalies near CTD17 might be linked to the anomalies further to the north of this area.

Both sections *B* and *C* have relatively weak turbidity anomalies of smaller than 0.025 ΔNTU at the depth of 2500—3000 m (Figure 6(b)). The turbidity anomalies are found from 24°07′S to 24°04′S (section *B*) and 24°02′S to 24°01′S (section *C*). The southern end of the anomaly section *D* is immediately to the south of a suggested plume site at 24°00.3′S, which was detected during Leg 2 of the 1988 GEMINO-3 cruise[11], while its northern end is at 23°55′S (Figure 6(b)). The turbidity plume layer is at a depth interval of 2600—3000 m and the maximum anomaly (greater than 0.04 ΔNTU) is located between 23°57′S and 23°56′S. The turbidity

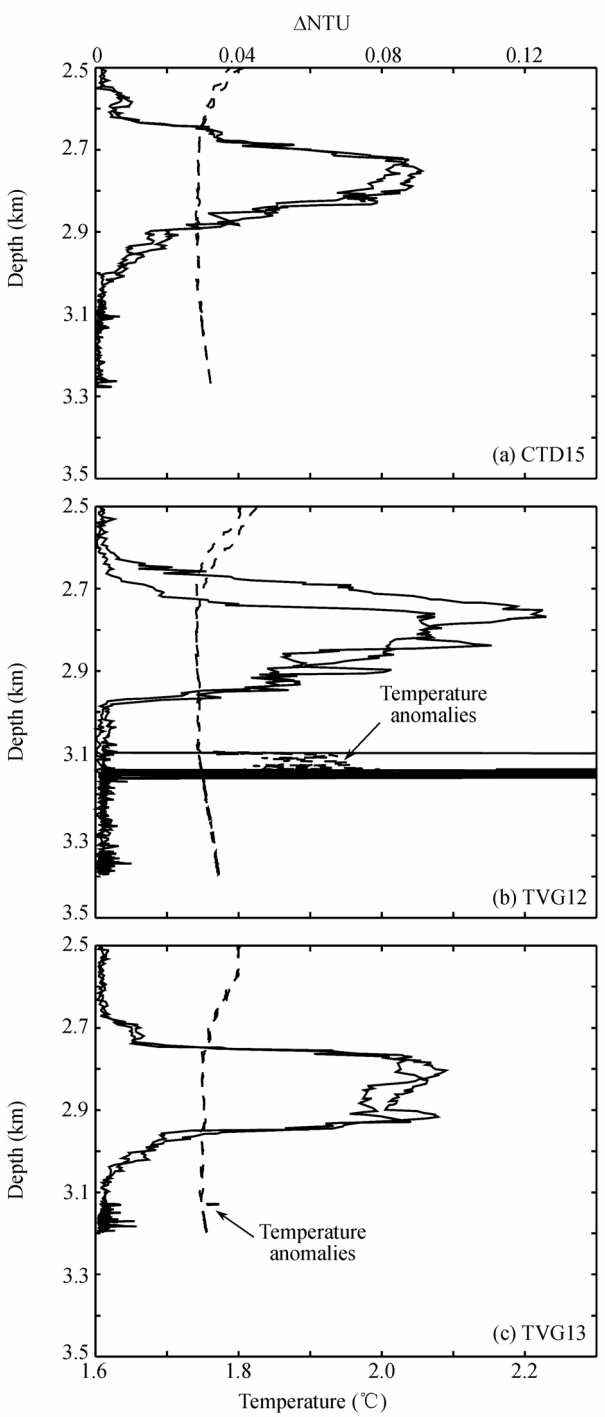

Figure 5 *In situ* MAPR station measurements near the Edmond vent field. The solid lines show the turbidity anomaly and the dashed lines show the temperature measurements. The black arrows in (b) and (c) indicate obvious temperature spikes at the depth from 3100 m to 3300 m. Sharp turbidity anomaly spikes also appear at the same depth in (b) and the maximum value is about 0.54 ΔNTU, which exceeds the turbidity scale of the horizontal axis.

anomaly reaches the maximum at the depth of 2700—2800 m, which is close to the depth range where maximum methane and manganese anomalies were observed

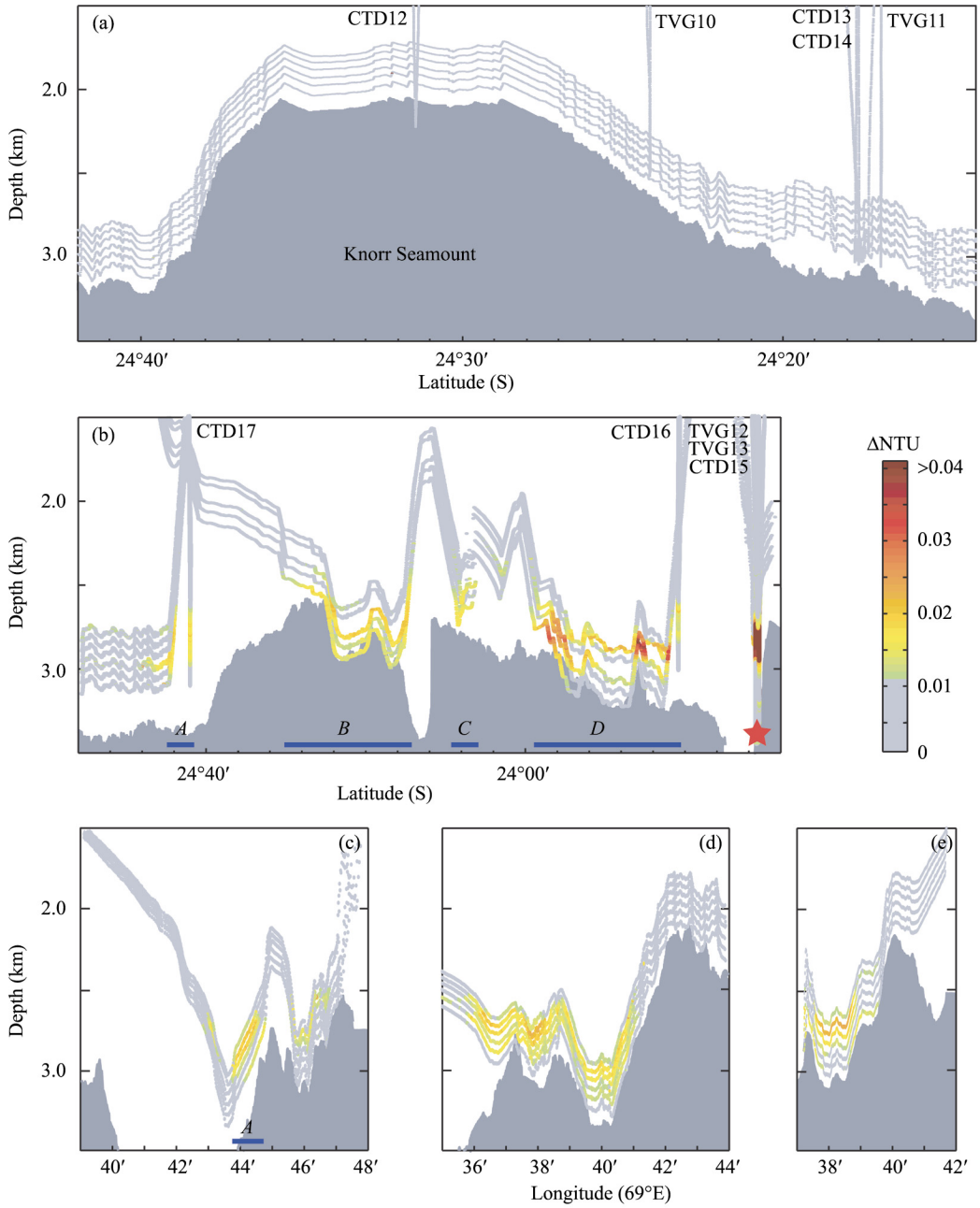

Figure 6 Near-bottom tow-yo MAPR tracks within the survey area. The gray shaded areas show the seafloor topo-graphy as determined by a shipboard SIMRAD multi-beam bathymetry system during our 2005 cruise. The color graphy as determined by a shipboard SIMRAD multi-beam bathymetry system during our 2005 cruise. The color ΔNTU is replaced by the light gray color, while values greater than 0.04 ΔNTU is saturated in red. (a) Turbidity values between 24°42′S and 24°14′S. (b) Turbidity values between 24°14′S and 23°52′S. The red star indicates the Edmond vent field. The blue bars with labels *A* —*D* indicate where significant turbidity anomalies were concentrated. (c)—(e) Turbidity values in three across-axis profiles.

during the 1988 GEMINO-3 cruise. Noticeable turbidity anomalies with magnitudes of less than 0.03 ΔNTU were also detected in two across-axis tow-yo profiles (Figure 6(d) and (e)), which were conducted between sections *C* and *D*. This northernmost across-axis profile (Figure 6(e)) was quite close to the Edmond vent field, and revealed strong anomaly with magnitude of 0.06 ΔNTU.

Figure 7 summarizes the turbidity anomaly distribution within the survey area in map view. The data for base topography map are again from the online open database (http://www.marine-geo.org/) and the contour interval is 400 m. The turbidity value shown for each location is the maximum turbidity value among the six

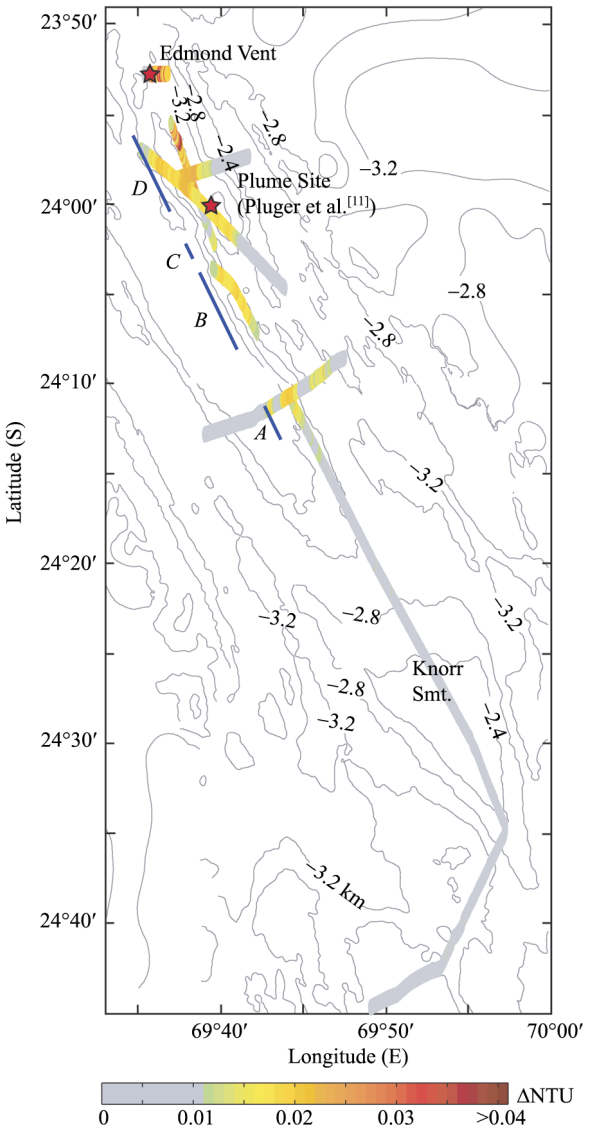

Figure 7 Map view of MAPR tow-yo measurements. The data are limited to where the sensors are within 1000 m above the seafloor. The two red stars show the Edmond vent field and an inferred hydrothermal vent field by Pluger et al.[11], respectively. The color scale is the same as that in Figure 6. Color for each location reflects the maximum turbidity anomaly value among the six MAPR sensors at that location. The data for base topography map are from http://www.marine-geo.org and the contour interval is 400 m. Labels *A*, *B*, *C*, and *D* indicate the same areas of noticeable anomalies as shown in Figure 6(b), but are projected onto the sensor track direction.

MAPR sensors at that location. Only the turbidity data within 1000 m above the seafloor are plotted. The color scale is the same as in Figure 6. The anomaly sections *A* to *D* have the same definition as in Figure 6(b), but are projected along the sensor track. The hydrothermal plume above the Edmond vent field extends about 4 km to the east. We note that the plumes in these four individual sections and at the Edmond vent filed are at similar water depth. If all the four sections (*A* to *D*) are connected to the Edmond hydrothermal plume, the total along-axis length of the plume anomaly would be more than 37 km. The resultant plume incidence p_h within the survey area, which is defined here as the length of the ridge axis with plume anomalies greater than 0.01 ΔNTU over the total surveyed ridge length, would be about 0.38. This value is 1.5 times as much as the predicted p_h of 0.21—0.25 for the spreading rate of 50—60 mm/a[12]. This suggests that this part of the Central Indian Ridge may be in a period of relatively robust hydrothermal activity.

4 Conclusions

(1) Strong hydrothermal plume anomalies were recorded over the previously discovered Kairei and Edmond vent fields, with the turbidity anomalies concentrated at depth intervals of 2150—2300 m and 2700—2900 m, respectively. The maximum height of the turbidity anomalies recorded in December 2005 above the Kairei vent field is similar to that recorded in June 2001, indicating that the Kairei hydrothermal vent field may have maintained its buoyancy flux during the intervening 4.5 years.

(2) There are background turbidity anomalies of about 0.005ΔNTU beneath the Kairei hydrothermal plume, but no such background anomalies were observed beneath the Edmond plume.

(3) No visible turbidity anomalies were detected from 24°42′S to 24°12′S including the Knorr Seamount. Thus 24°12′S marks the southern end of the hydrothermal plume.

(4) Significant turbidity anomalies at a depth interval of 2500—3000 m were detected from 24°12′S to 23°56′S along the eastern rift valley wall at four individual sections where the MAPR sensors have reached an appropriate depth range. Whether these individual sections of anomalies are partly or completely connected remains unknown due to the absence of data from the intervening gaps. If the four sections are indeed connected to the Edmond vent field farther to the north, then the total along-axis length of the plume anomaly would be more than 37 km. This would imply a plume incidence p_h of 0.38, greater than the predicted p_h of 0.21—0.25 based on the spreading rate of the Central Indian Ridge. This suggests that this part of the Central Indian

Ridge may be in a period of relatively robust hydrothermal activity.

We are grateful to Edward Baker for loaning NOAA's MAPR instruments and the science party and crew members of the DY105-17A cruise for dedicated and professional operation at sea. Thanks also to Chris German, Edward Baker, Richard Von Herzen, Ruixin Huang, Patricia Gregg, and Debbie Smith for valuable discussion and comments that have greatly improved this study and to Niu Yaoling (editor), Wolfgang Bach, and an anonymous reviewer for thorough reviews.

1 Gamo T, Chiba H, Yamanaka T, et al. Chemical characteristics of newly discovered black smoker fluids and associated hydrothermal plumes at the Rodriguez Triple Junction, Central Indian Ridge. Earth Planet Sci Lett, 2001, 193: 371－379[DOI]
2 Van Dover C L, Humphris S E, Fornari D, et al. Biogeography and ecological setting of Indian ocean hydrothermal vents. Science, 2001, 294: 818－823[DOI]
3 DeMets C, Gordon R G, Argus D F, et al. Current plate motions. Geophys. J Int, 1990, 101: 425－478[DOI]
4 Briais A. Structural analysis of the segmentation of the Central Indian Ridge between 20°30′S and 25°30′S. Mar Geophys Res, 1995, 17: 431－467[DOI]
5 Hashimoto J, Ohta S, Gamo T, et al. First hydrothermal vent communities from the Indian Ocean discovered. Zool Sci, 2001, 18: 717－721[DOI]
6 Gallant R M, Von Damm K L. Geochemical controls on hydrothermal fluids from the Kairei and Edmond Vent Fields, 23o-25oS, Central Indian Ridge. Geochem Geophy Geosyst, 2006, 7, doi: 10.1029/2005GC001067[DOI]
7 Canales J P, Danobeitia J J, Detrick R S, et al. Variations in axial morphology along the Galapagos spreading center and the influence of the Galapogos hotspot. J Geophys Res, 1997, 102: 27341－27354[DOI]
8 Baker E T, Milburn H.B. MAPR: A new instrument for hydrothermal plume mapping. RIDGE Events, 1997, 8: 23－25
9 Rudnicki M D, German C R. Temporal variability of the hydrothermal plume above the Kairei vent field, 25oS, Central Indian Ridge. Geochem Geophys Geosyst, 2002, 3, doi:10.1029/2001GC000240[DOI]
10 Turner J S. Buoyancy Effects in Fluids. Cambridge: Cambridge University Press, 1973. 368
11 Pluger W L, Herzig P M, Becker K P, et al. Discovery of Hydrothermal Fields at the Central Indian Ridge. Mar Min, 1990, 9: 73－86
12 Baker E T, Edmonds H N, Michael P J, et al. Hydrothermal venting in magma deserts: The ultraslow-spreading Gakkel and Southwest Indian Ridges. Geochem Geophys Geosyst, 2004, 5, doi: 10.1029/2004GC000712[DOI]